

# MRI-Based Computational Hemodynamics in Patients

Andreas Ruopp and Ralf Schneider

**Abstract** The target of this research was to develop a simulation process chain for the analysis of arterial hemodynamics in patients with automatic calibration of all boundary conditions for the physiological correct treatment of flow rates in transient blood flows with multiple bifurcations. The developed methodology uses stationary simulations at peak systolic acceleration and minimizes the error of target and simulated outflow conditions by means of a parallel genetic optimization approach. The target inflow and outflow conditions at peak systole are extracted from 4D phase contrast magnetic resonance imaging (4D PC-MRI). The flow resistance of the arterial system lying downstream of the simulation domain's outlets is modelled via porous media with velocity dependent loss coefficients. In the analysis of the subsequent transient simulations, it will be shown that the proposed calibration method shows to work suitable for three different types of patients including one healthy patient, a patient suffering from an aneurysm as well as one with a coarctation. Additionally the local effects of mapping the measured transient 4D PC-MRI data onto the aortic valve inlet in comparison to the usage of block inlet profiles will be shown.

## 1 Introduction

Computational fluid dynamics (CFD) can help to visualize and understand the flow behaviour in the human arterial system. Nowadays, patient specific CFD models are created from MRI or computer tomography (CT) in order to get realistic geometries and to evaluate pressure gradients in regions of coarctations [6, 9]. In future, CFD methods will help to reduce the need for diagnostic catheterization. In this context, new studies treat both pre- and post-treatment in CFD studies to improve their accuracy based on real patient data [5, 10]. Generally, 4D-MRI data are used to obtain the flow rates in the ascending and descending aorta. All other outlets in between are treated according to methods which rely on cross-sectional area relationships [5, 8]. The simulations have in common, that outflow conditions with

---

A. Ruopp (✉) • R. Schneider  
HLRS, University of Stuttgart, Nobelstrasse 19, 70569 Stuttgart, Germany  
e-mail: [ruopp@hlrs.de](mailto:ruopp@hlrs.de); [schneider@hlrs.de](mailto:schneider@hlrs.de)

fixed flow rates are identical for both pre- and post-treatment setups even though the flow resistance in the arteries under consideration might be significantly altered by e.g. angioplasty.

This paper deals with the correct utilization of outflow conditions, when flow rates can be extracted from measurements via MRI. In this case, fluxes would be patient based and outflow conditions are calibrated to each single patient in order to use Dirichlet conditions for pressure at all outlets in conjunction with velocity dependent loss coefficients of porous media. By this approach the flow resistance of the arterial system lying downstream of each outlet is modelled independently from the flow conditions in the simulation domain.

## 2 Methodology

The following section gives an overview about the applied CFD codes, the complete optimization chain as well as the meshing, the domain mapping and the treatment of stationary and transient boundary conditions. The established work flow shows to be valid for different cases of hemodynamics in patients. Additionally, the use of porous domains clearly stabilizes the solution procedure and suppresses pressure reflections in the beginning of transient runs leading to higher possible Courant numbers for implicit solvers.

### 2.1 Geometries

In this study, we use three different types of arterial systems originating just behind the aortic valve with different numbers of bifurcations, see Fig. 1. Case a was

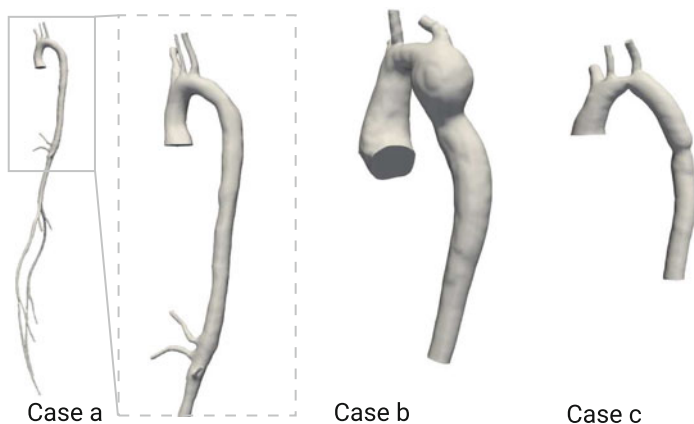


**Fig. 1** Three hemodynamic cases. a—Healthy patient, b—patient with aneurysm and c—patient with coarctation. All geometries in same scale except total view of a

extracted from CT while b and c are both extracted using PC-MRI data. Case b and c are inherited from Mirzaee et al. [10]. Case a consists of one inlet and thirteen outlets while case b and c have four outlets in total.

The edge resolution of the stereolithographic representation of case a and c is in the range of 0.0001 [m] for the most curved parts. Case b uses a higher resolution down to  $10^{-6}$  [m]. All inlet and outlets are cut almost perpendicular with respect to the aortic wall in order to avoid numerical errors.

## 2.2 Meshing

We use a cartesian based meshing process *cartesianMesh* from cfMesh [2] for all three setups. One key advantage of this mesher is the fully automated workflow via scripting. Table 1 highlights the meshing parameters for each geometry setup. At each outlet, we introduce an additional volume mesh where the boundary mesh is extruded perpendicular to face normal's with ten layers each and an average thickness of about 0.0025 [m] per layer, see Fig. 2. The extrusion is done with the utility *extrudeMesh* which is included in the framework *OpenFOAM*<sup>®</sup>. In addition, each extruded mesh is marked with a *cellZone* being able to introduce specific source terms for porous media treatment during the simulation run.

**Table 1** Meshing parameters for *cfMesh*

Parameter	Case		
	a	b	c
Maximum cell size [m]	0.001	0.001	0.001
Refinement size of aortic wall [m]	0.0005	0.001	0.0005
Number of layers	3	2	2
Refinement of outlets [m]	0.0005–0.00025	0.001	0.0005
Cell numbers	1,083,243	350,061	347,391

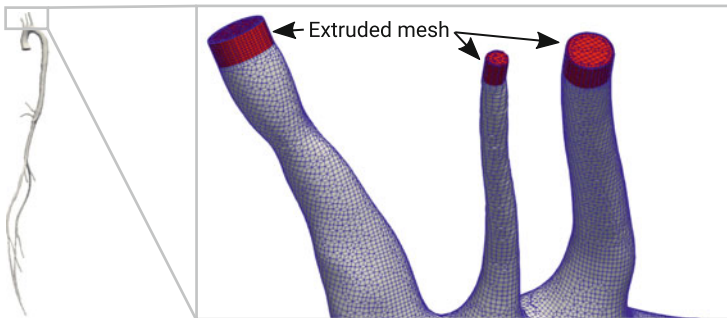


**Fig. 2** Extruded meshes at outlets for case a needed in conjunction with porous media. Grey color show mesh creation with *cfMesh*, red color indicates the extruded mesh afterwards

### 2.3 CFD Setup

Two CFD setups are performed including a steady state simulation setup for the optimization process followed by a transient case study. We assume, that the blood flow can be treated as in-compressible fluid behaviour. Therefore, we solve the steady and the unsteady Navier-Stokes equations in the following form

$$\frac{\partial \mathbf{U}}{\partial t} + (\mathbf{U} \cdot \nabla) \mathbf{U} - \nu \nabla^2 \mathbf{U} = -\frac{1}{\rho} \nabla p + S \quad (1)$$

$$\nabla \cdot \mathbf{U} = 0 \quad (2)$$

with  $\nabla$  the Nabla operator, velocity  $\mathbf{U}$ , viscosity  $\nu$ , time  $t$ , pressure  $p$ , density  $\rho$  and a source term  $S$ , using the solvers *simpleFoam* and *pimpleFoam* from *OpenFOAM*® Version 2.4.x respectively.

The porous media is introduced as a source term  $S$ , where we use an explicit porosity source *explicitPorositySource* with Darcy-Forchheimer model and the following relation

$$S = -\rho C_0 |\mathbf{U}|^{(C_1-1)} \mathbf{U} \quad (3)$$

$C_0 \equiv$  Model linear coefficient

$C_1 \equiv$  Model Exponent coefficient

with a fixed value of  $C_1 = 2$  and a variable value of  $C_0$  which has to be determined by optimization.

The boundary conditions are listed in Table 2 where  $\nu_t$  denotes the turbulent viscosity of the fluid. We apply the *kOmegaSST*-model for all runs with a fixed

**Table 2** Boundary conditions for steady state and transient runs for all three cases

	Inlet aortic valve	Outlet	Aortic wall
<i>Steady state</i>			
$\nu_t$	calculated	calculated	nutkWallFunction
$k$	fixedValue	zeroGradient	kqRWallFunction
$p$	zeroGradient	fixedValue	zeroGradient
$\omega$	fixedValue	zeroGradient	omegaWallFunction
$\mathbf{U}$	fixedValue	zeroGradient	fixedValue
<i>Transient</i>			
$\nu_t$	calculated	calculated	nutkWallFunction
$k$	groovyBC	groovyBC	kqRWallFunction
$p$	zeroGradient	fixedValue	zeroGradient
$\omega$	groovyBC	groovyBC	omegaWallFunction
$\mathbf{U}$	groovyBC (case a) timeVaryingMappedFixedValue (case b,c)	zeroGradient	fixedValue

kinematic viscosity of  $0.004 \cdot 10^{-03} \text{ m}^2/\text{s}$  and impose a fixed value for  $k$  and  $\omega$  at the aortic inlet with the following relations

$$k = 1.5 \cdot (|\mathbf{U}| \cdot I)^2 \quad (4)$$

$$I = 1 \text{ [%]} \quad (5)$$

$$\omega = 0.09 \cdot \frac{\sqrt{k}}{r_{\text{hydraulic}}} \quad (6)$$

$$r_{\text{hydraulic}} = \sqrt{\frac{A_{\text{Inlet}}}{\pi}} \quad (7)$$

and a regular block profile for the velocity. For the transient cases, we apply a variable boundary condition that can switch between Dirichlet and Neumann dependent on the sign of the flux  $\Phi_f$  at every boundary face. For  $\Phi_f < 0$  the following values are set for  $k$  and  $\omega$  at each face

$$k = 1.5 \cdot (|\mathbf{U}_f| \cdot I)^2 \quad (8)$$

$$\omega = \max \left( 0.09 \cdot \frac{\sqrt{k_f}}{r_{\text{hydraulic}}} \right) \quad (9)$$

where the subscript  $f$  denotes the position of the considered face's centre. For  $\Phi_f \geq 0$  we impose a zero gradient condition for  $k$  and  $\omega$  at each face.

The flow rate over time, given in Fig. 3, results in  $5.1 \left[ \frac{1}{\text{min}} \right]$  for case a (inlet condition is similar to [11]),  $5.35 \left[ \frac{1}{\text{min}} \right]$  for case b and case c leads to  $4.51 \left[ \frac{1}{\text{min}} \right]$ . For case b and c the measured velocity profiles, extracted from the according PC-MRI data were used at the inlet. The velocity vectors were interpolated in space and time onto the CFD mesh resulting in a more realistic inlet condition compared to

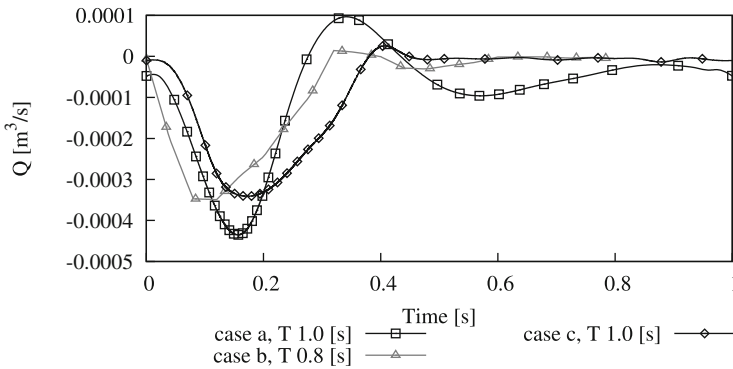


**Fig. 3** Given flow rate over time at inlet for case a, b and c

case a, see Fig. 4. Due to the turbulent velocity profile the flux dependent boundary condition at each cell face via *groovyBC* was needed.

No patient specific flow rates over time were available for case a at each outlet which is crucial for a correct calibration of entire hydrodynamic system. This also stands true for case b and c, since the evaluation of the 4D PC-MRI measurement data at each outlet violates the continuity equation with peak errors above 100 [%]. For this reason, we assume specific flow rates, derived from literature, which are summarized in Table 3. The target flow rates of all outlets for case a are given in Table 4 as well as for case b and c (Table 5) in terms of percentage of flow rate at inlet. We assume, that the given fractions stay constant during one heart beat.

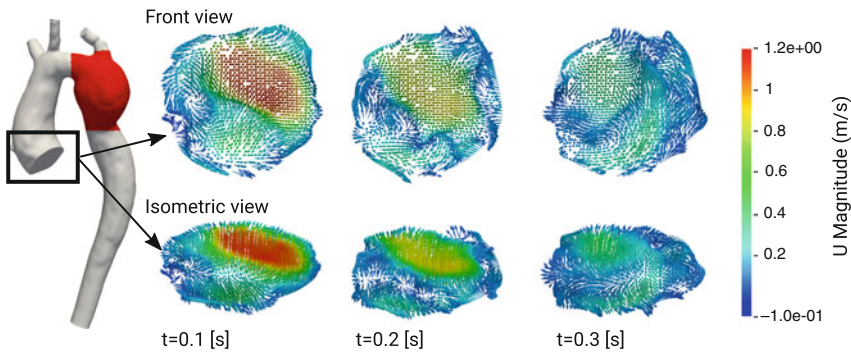


**Fig. 4** Velocity vectors at aortic inlet for case b in front view (*upper row*) and isometric view (*lower row*), *color* indicating magnitude of velocity. Aneurysm section colored *red* in geometry (*left picture*)

**Table 3** Division of volumetric flux at different bifurcations for case a, based on [13] (MiZ) and [7] (BWP)

Classification	Weight [kg]	Fraction [%]	BWP [ $\frac{1}{\text{min}}$ ]	Fraction [%]	MiZ [ $\frac{1}{\text{min}}$ ]	Fraction [%]	[ $\frac{1}{\text{min}}$ ]	Average [%]
Abdomen	2.8	4.0	1.4	24.1	–	21	–	22.6
Kidneys	0.3	0.4	1.1	19.0	–	23	–	21.0
Brain	1.5	2.1	0.75	12.9	–	15	–	14.0
Heart	0.3	0.4	0.25	4.3	–	5	–	4.7
Skeleton muscles	30.0	42.9	1.2	20.7	–	17	–	18.8
Skin	5.0	7.1	0.5	8.6	–	8	–	8.3
Other organs	30.1	43.0	0.6	10.3	–	4	–	10.7
Liver	–	–	–	–	–	7	–	–
Sum	70.0	100.0	5.8	100.0	4.9	100	5.35	100.0

Missing data marked with –

**Table 4** Division of volumetric flux at different bifurcations for case a, based on [13] (MiZ) and [7] (BWP)

	Flow rate [ $\frac{1}{\text{min}}$ ]	Fraction of inlet [-]
Inlet	5.101	1.000
Truncus Brachiocephalicus 03	0.549	0.108
Arteria Carotis Communis 02	0.072	0.014
Arteria Subclavia 01	0.331	0.065
Truncus Coeliacus 04	1.202	0.236
Arteria Mesenterica Superior 05	1.202	0.236
Arteria Renalis Sinistra 06	0.561	0.110
Arteria Renalis Dextra 07	0.561	0.110
Arteria Iliaca Interna L 08	0.105	0.021
Arteria Iliaca Interna R 09	0.105	0.021
Arteria Profunda Femoris L 10	0.105	0.021
Arteria Profunda Femoris R 11	0.105	0.021
Arteria Femoralis L 12	0.102	0.020
Arteria Femoralis R 13	0.102	0.020

**Table 5** Division of volumetric flux at different bifurcations for case b and c, based on [13] (MiZ) and [7] (BWP)

	Flow rate [ $\frac{1}{\text{min}}$ ]	Frac. of inlet [-]	Flow rate [ $\frac{1}{\text{min}}$ ]	Frac. of inlet [-]
Inlet	5.350	1.000	4.510	1.000
Arteria Subclavia 01	0.327	0.061	0.275	0.061
Arteria Carotis Communis 02	0.245	0.046	0.207	0.046
Truncus Brachiocephalicus 03	0.381	0.071	0.321	0.071
Outlet 04	4.397	0.822	3.707	0.822

## 2.4 Optimization Workflow

We apply an optimization workflow according to [12] for the steady state simulation runs in order to obtain the correct loss coefficient  $C_0$  at each outlet. The optimization algorithm is identical to [4] which uses an evolutionary approach.

Case a uses in total 52 individuals per generation, case b and c 16 individuals. All loss coefficients were allowed to vary between  $0.01-9 \cdot 10^6$ . The optimization run strives for the minimum of the sum of each error between target flow rates and simulated flow rates

$$\epsilon = \sum_{i=1}^{n_{\text{outlets}}} \frac{\delta_i - \delta_{\text{target},i}}{\delta_{\text{target},i}} \quad (10)$$

### 3 Results

The following chapter shows the optimization results and the computational effort to calibrate systems with 13 or four unknowns respectively. Specific flow rates over time for different outlet sections and velocity distributions at different positions compared to the measured velocity field are presented for case b.

#### 3.1 Optimization Results

In total, 10,000 designs had to be evaluated for case a, see Fig. 5, which takes 72 [h] using 1248 cores simultaneously on the HLRS Hazel Hen [3] system. Case b and case c, Fig. 6, with four outlets each need at least 300 and 1400 design evaluations respectively using 384 cores with a total time of at least 4 and 16 [h].

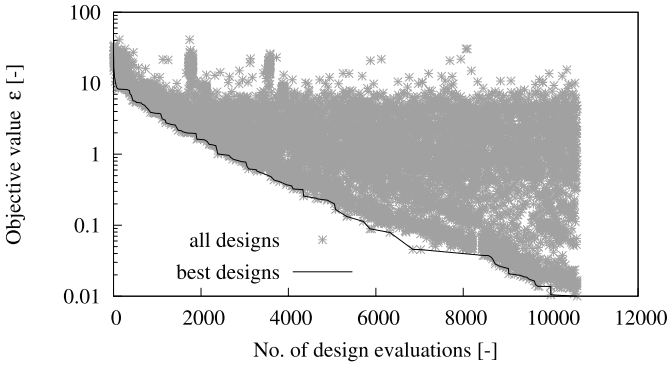


Fig. 5 Objective value  $\epsilon$  over number of simulation runs (individuals) for case a

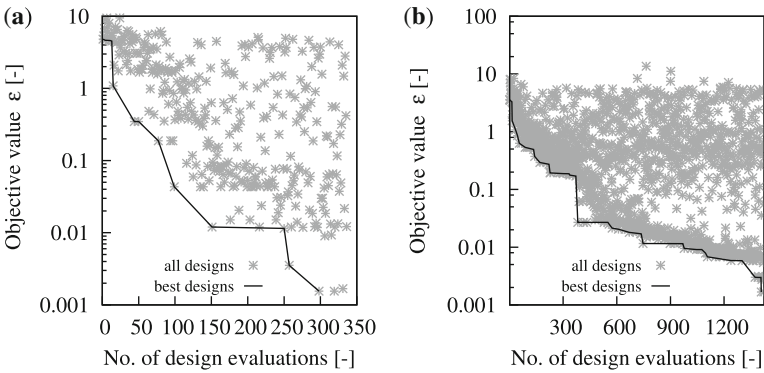


Fig. 6 Objective value  $\epsilon$  over number of simulation runs (individuals) for (a) case b and (b) case c



### 3.2 Global Target Values

The difference of volumetric fluxes over time for the calibrated and uncalibrated transient run for one heart beat is shown in Fig. 7. A calibration phase is necessary to obtain sensible fluxes over time. In addition, the presented porous media technique along with the shown calibration enables the simulation of one heart beat from rest. Without calibration and transient pressure boundary conditions at the outlets, one needs to simulate at least four heart beats to obtain a periodic transient state. This holds also true for case a and case b with a smaller number of outlets.

### 3.3 Local Variations

The local variations in magnitude of velocity are shown in Figs. 8, 9, and 10. The simulation run with calibrated outlets and correct mapped velocity field at the aortic inlet gives a relative good quantitative result. The uncalibrated run fails to capture

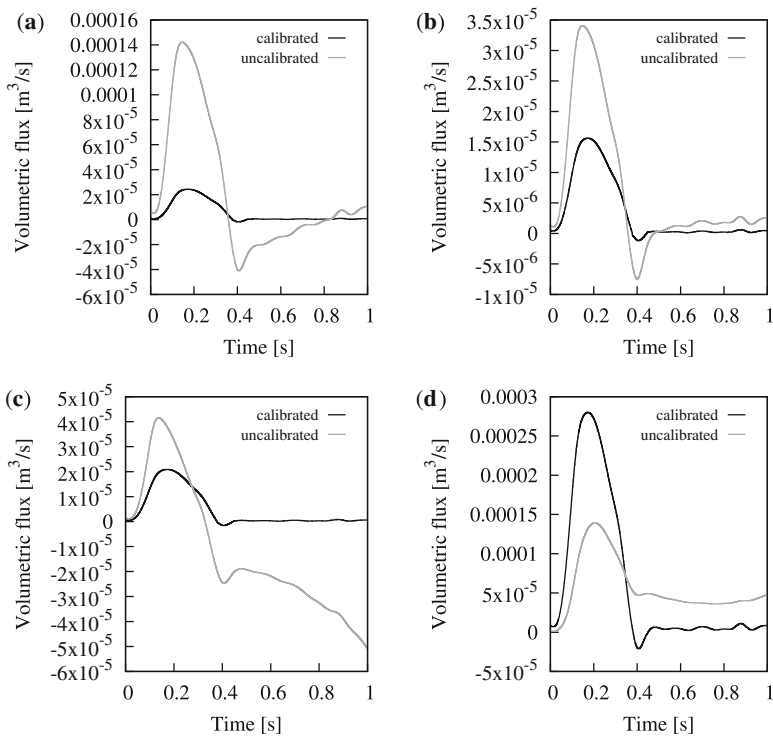


**Fig. 7** Volumetric fluxes over time at all four outlets for case c for first heart beat. (a) Outlet 01. (b) Outlet 02. (c) Outlet 03. (d) Outlet 04

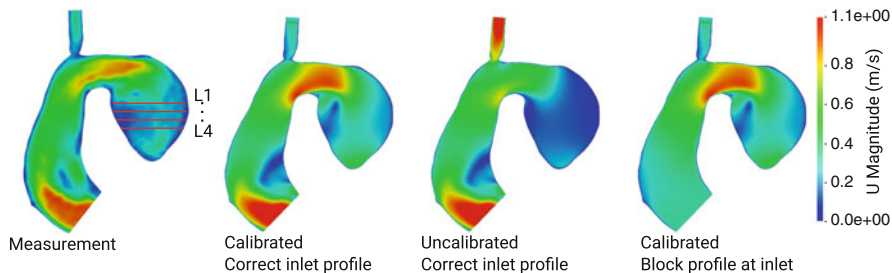


**Fig. 8** Magnitude of velocity on slice through middle of aneurysm section of case b. *From left to right*: PC-MRI measurement, the calibrated run with correct inlet condition (from measurement), the uncalibrated run with correct inlet condition and calibrated run with a block profile at inlet at  $t = 0.12$  [s]. *Lines* (L1–L4) indicate probing position for quantitative comparison, see Appendix with Figs. 11 and 12

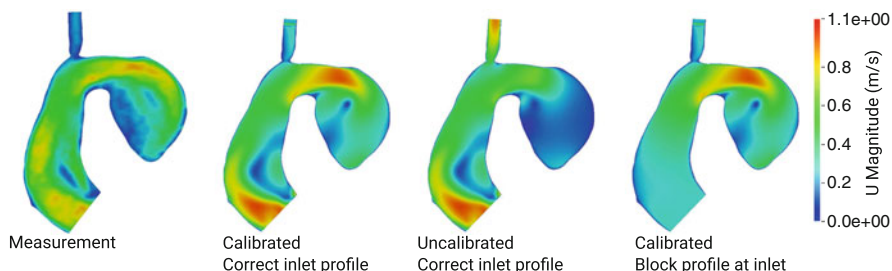


**Fig. 9** Magnitude of velocity on slice through middle of aneurysm section of case b. *From left to right*: PC-MRI measurement, the calibrated run with correct inlet condition (from measurement), the uncalibrated run with correct inlet condition and calibrated run with a block profile at inlet at  $t = 0.16$  [s]

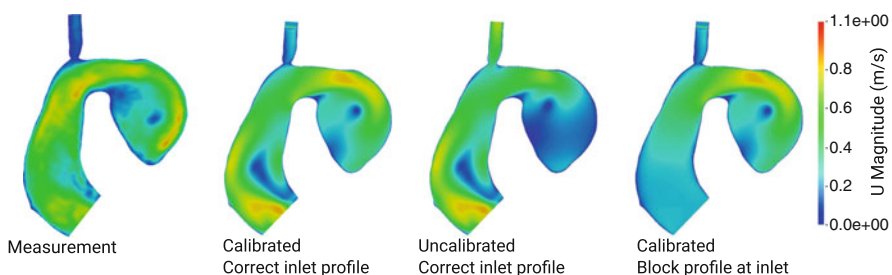


**Fig. 10** Magnitude of velocity on slice through middle of aneurysm section of case b. *From left to right*: PC-MRI measurement, the calibrated run with correct inlet condition (from measurement), the uncalibrated run with correct inlet condition and calibrated run with a block profile at inlet at  $t = 0.20$  [s]

correctly the swirling flow field in the aneurysm section due to an unphysiological high volumetric flux in the region of the *Arteria Subclavia*. The calibrated run with the wrong inlet condition produces valid results behind the arch but the region next to the inlet is not captured correctly. In addition, the velocity distribution along four lines in the aneurysm section is shown in Figs. 11 and 12 again for the identical time steps. This quantitative comparison clearly shows a mismatch between the measurements and the simulation because the PC-MRI data (MRT) does have some inaccuracy according to each velocity component in dependency of the position. In addition, the simulation neglects fluid-structure interactions as well as detailed roughness estimations of aortic walls.

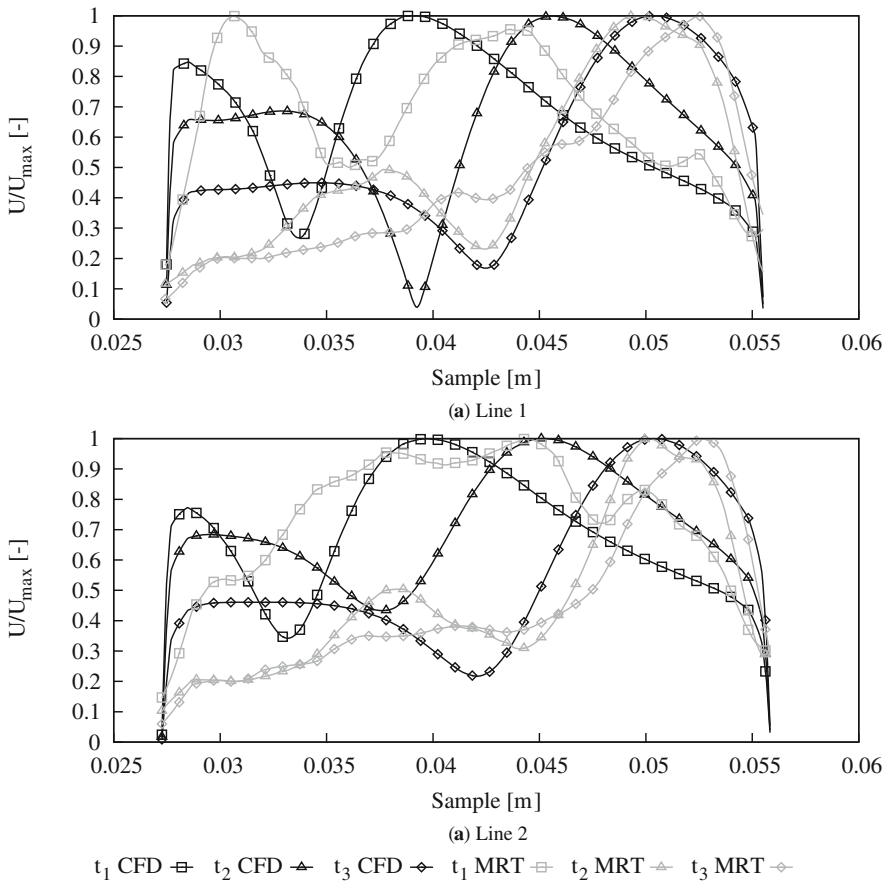


**Fig. 11** Quantitative comparison of magnitude of velocity along sampling lines (line definition see Fig. 8) (a) for line 1 (L1) and (b) for line 2 (L2)

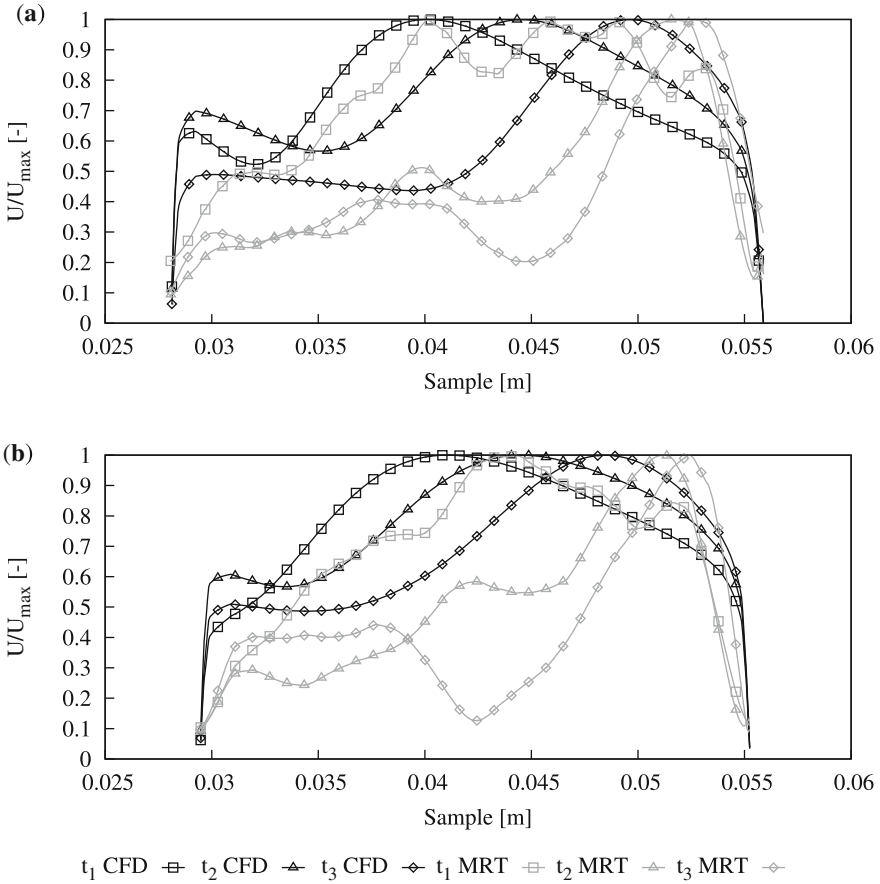


**Fig. 12** Quantitative comparison of magnitude of velocity along sampling lines (line definition see Fig. 8) (a) for line 3 (L3) and (b) for line 4 (L4)

### 3.4 Performance Issues

In order to get reasonable insights into the flow patterns of such types of hemodynamics as represented by case b and c, one has to utilize at least 1560 [Coreh]. The pre-treatment of patient specific data such as the extraction of geometry as STL representation is not included. All twelve cases from [10] with pre and post treatment of patients would need at least  $\approx 19,065$  [Coreh] with the introduced scheme including optimization and transient run.

To estimate case counts that could be expected if the methodologies described above should be applied to indications found in typical cohort sizes, which are regarded as reasonable in classical clinical studies, we consider the cases described above. In average cohort sizes, we consider  $\approx 5500$  individuals (extracted

from [1, 14]) with an average prevalence of 7.3 [%] of the regarded indication. This as a basis for further resource estimations of virtual clinical trials (see also [15]) leads to  $\approx 400$  individuals to which the simulation process has to be applied. If one takes into account one optimization to the preoperative state in conjunction with one preoperative and at least three postoperative transient evaluations in total, at least 656,000 [Coreh] are needed. This number of core-hours is the equivalent of 1 [day] facilitation of 1140 nodes on the HLRS Hazel Hen system [3].

## 4 Conclusion

Three patient specific geometries are simulated in a fully automated simulation process chain. The boundary conditions are treated with porous media with velocity dependent loss coefficients that are calibrated to physiological flow rates. By means of a parallel optimization process, aortic systems with up to 13 outlets can be calibrated in an adequate time. The transient simulation results clearly show the need of fully transient boundary conditions at the inlet, which have to be mapped from measurements in space and time. This enables a qualitative correct flow field in the complete domain in contrast to other assumptions such as block or parabolic profiles. At the moment, the lack of correct extraction of volumetric fluxes over time at each outlet for the target criteria is overcome by use of physical sensible estimations. Fixed pressure values at outlets in conjunction with the porous media model, even in varying conditions over time, can reproduce the correct flux balance.

In the sense of virtual clinical trials, an adequate number of individuals need to be investigated leading to a not insignificant usage of HPC systems. The presented estimation does not include fluid-structure interactions and non-Newtonian fluids.

## Appendix

See Figs. 11 and 12.

## References

1. Alcorn, H.G., Wolfson, S.K., Sutton- H., O'Leary, D.: Risk factors for abdominal aortic aneurysms in older adults enrolled in the cardiovascular health study. *Arterioscler. Thromb. Vasc. Biol.* **16**, 963–970 (1996)
2. cfMesh, <http://cfmesh.com/>, 14 Sept 2015
3. Cray XC40 (Hazel Hen). <http://www.hlrs.de/systems/cray-xc40-hazel-hen/>, May 2017
4. Deb, K., Tiwari, S.: Omni-optimizer: a generic evolutionary algorithm for single and multi-objective optimization. *Eur. J. Oper. Res.* **185**, 1062–1087 (2008)

5. Goubergrits, L., Riesenkampff, E., Yevtushenko, P., Schaller, J., Kertzscher, U., Hennemuth, A., Berger, F., Schubert, S., Kuehne, T.: MRI-based computational fluid dynamics for diagnosis and treatment prediction: clinical validation study in patients with coarctation of aorta. *J. Magn. Reson. Imaging* **41**, 909–916 (2015)
6. LaDisa, J.F., Alberto Figueroa, C., Vignon-Clementel, I.E., Jin Kim, H., Xiao, N., Ellwein, L.M., Chan, F.P., Feinstein, J.A., Taylor, C.A.: Computational simulations for aortic coarctation: representative results from a sampling of patients. *J. Biomech. Eng.* **133**, 091008–091008-9 (2011)
7. Lang, F., Lang, P.: *Basiswissen Physiologie*. 2nd edn. Springer, Berlin, Heidelberg (2007). <http://dx.doi.org/10.1007/978-3-540-71402-6>. ISBN:978-3-540-71402-6
8. Lantz, J., Karlsson, M.: Large eddy simulation of LDL surface concentration in a subject specific human aorta. *J. Biomech.* **45**, 537–542 (2012)
9. Menon, P.G., Pekkan, K., Madan, S.: Quantitative hemodynamic evaluation in children with coarctation of aorta: phase contrast cardiovascular MRI versus computational fluid dynamics. In: *Statistical Atlases and Computational Models of the Heart. Imaging and Modelling Challenges: Third International Workshop, STACOM 2012, Held in Conjunction with MICCAI 2012, Nice, October 5 (2012). Revised Selected Papers*. Camara, O., Mansi, T., Pop, M., Rhode, K., Sermesant, M. Young, A. (eds.), pp. 9–16. Springer, Berlin, Heidelberg (2013)
10. Mirzaee, H., Henn, T., Krause, M.J., Goubergrits, L., Schumann, C., Neugebauer, M., Kuehne, T., Preusser, T., Hennemuth, A.: MRI-based computational hemodynamics in patients with aortic coarctation using the lattice Boltzmann methods: clinical validation study. *J. Magn. Reson. Imaging* **45**, 139–146 (2017)
11. Patel, N., Küster, U.: Geometry dependent computational study of patient specific abdominal aortic aneurysm. In: Resch, M.M., Bez, W., Focht, E., Kobayashi, H., Patel, N. (eds.) *Sustained Simulation Performance 2014. Proceedings of the Joint Workshop on Sustained Simulation Performance*, University of Stuttgart (HLRS) and Tohoku University, pp. 221–238. Springer International Publishing, New York (2015)
12. Ruopp, A., Ruprecht, A., Riedelbauch, S.: Automatic blade optimisation of tidal current turbines using OpenFOAM<sup>®</sup>. In: *9th European Wave and Tidal Energy Conference (EWTEC)*, Southampton (2011)
13. Schaal, S., Steffen, K., Konrad, K.S.: *Der Mensch in Zahlen: Eine Datensammlung in Tabellen mit über 20000 Einzelwerten*, 4th edn. Springer Spektrum, Berlin (2016). <http://dx.doi.org/10.1007/978-3-642-55399-8>. ISBN:978-3-642-55399-8
14. Singh, K., Bønaa, K.H., Jacobsen, B.K., Bjørk, L., Solberg, S.: Prevalence of and risk factors for abdominal aortic aneurysms in a population-based study the Tromsø study. *Am. J. Epidemiol.* **154**, 236 (2001)
15. Viceconti, M., Henney, A., Morley-Fletcher, E.: *In silico clinical trials: how computer simulation will transform the biomedical industry. Research and Technological Development Roadmap*, Technical Report, 26 Mar 2017. <http://dx.doi.org/10.13140/RG.2.1.2756.6164>